AIP | Journal of Applied Physics

Graphene formation on step-free 4H-SiC(0001)

M. L. Bolen, R. Colby, E. A. Stach, and M. A. Capano

Citation: J. Appl. Phys. **110**, 074307 (2011); doi: 10.1063/1.3644933
View online: http://dx.doi.org/10.1063/1.3644933
View Table of Contents: http://jap.aip.org/resource/1/JAPIAU/v110/i7
Published by the AIP Publishing LLC.

Additional information on J. Appl. Phys.

Journal Homepage: http://jap.aip.org/
Journal Information: http://jap.aip.org/about/about_the_journal
Top downloads: http://jap.aip.org/features/most_downloaded
Information for Authors: http://jap.aip.org/authors

ADVERTISEMENT

Downloaded 18 Jul 2013 to 128.46.221.64. This article is copyrighted as indicated in the abstract. Reuse of AIP content is subject to the terms at: http://jap.aip.org/about/rights_and_permissions

Graphene formation on step-free 4H-SiC(0001)

M. L. Bolen,[1,2,a)] R. Colby,[2,3,b)] E. A. Stach,[4] and M. A. Capano[1,2,c)]
[1]*School of Electrical and Computer Engineering, Purdue University, West Lafayette, Indiana 47907, USA*
[2]*Birck Nanotechnology Center, Purdue University, West Lafayette, Indiana 47907, USA*
[3]*School of Materials Engineering, Purdue University, West Lafayette, Indiana 47907, USA*
[4]*Brookhaven National Laboratory, Upton, New York 11973, USA*

(Received 26 April 2011; accepted 15 August 2011; published online 5 October 2011)

Step-free SiC was thermally decomposed in vacuum to better understand graphene formation in the absence of step fronts. Atomic force microscopy revealed graphene nucleating at surface pits that preferentially form along SiC$\{1\bar{1}00\}$ planes. The density of these pits is $1\times10^8\text{cm}^{-2}$, which is three orders of magnitude greater than the measured density of SiC threading dislocations. Additionally, Raman spectroscopy demonstrated that graphene on step-free regions have a redshifted 2D peak position and a smaller peak width than does graphene grown on stepped regions. This difference is attributed to film thickness, which is confirmed by cross-sectional transmission electron microscopy. Stepped regions have a graphitic film nearly 2 nm thick as compared to less than 0.7 nm for step-free regions. © *2011 American Institute of Physics*. [doi:10.1063/1.3644933]

I. INTRODUCTION

The use of thermal decomposition to create graphitic films on a SiC surface has been known for over 30 years.[1] However, it has only been in recent years that research to use this technique to reliably create atomically thin graphite, known as graphene, has dramatically increased. Graphene formed on SiC has successfully served as a substrate for many different types of electronic devices,[2–4] but regardless of the end purpose, all research on SiC thermal decomposition has begun on a vicinal SiC substrate. A pristine, vicinally offcut SiC surface is characterized by a terraced surface morphology, with the width of terraces depending on the degree of offcut. This terraced surface naturally occurs because of the different surface energies of the basal plane stacking in the commonly used 4H- and 6H-SiC polytypes.[5] During the thermal decomposition of SiC, it has been found that the terrace step fronts, i.e., ledges, are the first features to begin to decompose.[6–10] This step front erosion appears to be a common growth phenomenon, regardless of the thermal decomposition environments studied to date, including various vacuum regimes and argon at near-atmospheric pressures. The cause of this initial step erosion can be understood through the Terrace-Ledge-Kink model.[11] Since the ledges are a higher surface energy feature, as compared to terraces, the ledges begin to decompose before the terrace. This raises a question: how does thermal decomposition proceed on a step-free SiC substrate? For the first time, experiments have been carried out and their results are presented to answer this question.

a)Now at National Renewable Energy Laboratory, Golden, Colorado 80401, USA.
b)Now at Pacific Northwest National Laboratory, Richland, Washington 99352, USA.
c)Electronic mail: capano@purdue.edu.

II. EXPERIMENTAL PROCEDURE

The starting substrate material is n-type 4H-SiC from Cree with an 8 degree miscut toward the SiC $\langle 11\bar{2}0\rangle$ direction. After e-beam evaporation of a protective metal mask, standard photolithography and wet-etching is used to pattern metallic circles across the SiC surface, with diameters ranging from 50 μm to 400 μm. Dry reactive ion etching (RIE) with SF_6 is used to pattern the circles into "mesas," which are embossed SiC pillars standing above the sample floor by nearly 10 μm. This height is found to be sufficient to prevent overgrowth from the SiC floor onto the top of the mesas during homoepitaxial growth. The mesas are separated from each other by at least 50 μm on all sides, and there are nearly 4×10^3 mesas per cm^2. After the metal mask is removed, the samples are loaded into an Epigress VP508 hot-wall chemical vapor deposition (CVD) reactor. Ten minutes of etching in a 1500 °C reactive hydrogen environment is used to remove any remaining surface scratches left from chemo-mechanical polishing and form a pristine SiC surface with terraces approximately 30 nm wide. Then, homoepitaxial step-flow growth is performed. The chamber pressure is maintained at 100 mbar with a growth temperature of 1600 °C for 60 min while flowing 30 slm of H_2 as a carrier gas and 3 sccm of C_3H_8 and 6 sccm of SiH_4 as precursor gases. Under these conditions, the mesa ledges grow forward together in a relatively uniform, lock-step manner until each individual ledge has reached the edge of the mesa. The last ledge to grow across the entire mesa leaves behind a step-free surface when it terminates at the edge of the mesa. In this fashion, a step-free surface can be obtained over hundreds of square micrometers.[12]

If there is not sufficient growth time for the last ledge to completely cover the mesa surface, then the mesa becomes only partially covered with a step-free region. A cartoon representation of the step-flow growth process is shown in Fig. 1. The dry-etched substrate, with a mesa embossed

 © 2011 American Institute of Physics

Downloaded 18 Jul 2013 to 128.46.221.64. This article is copyrighted as indicated in the abstract. Reuse of AIP content is subject to the terms at: http://jap.aip.org/about/rights_and_permissions

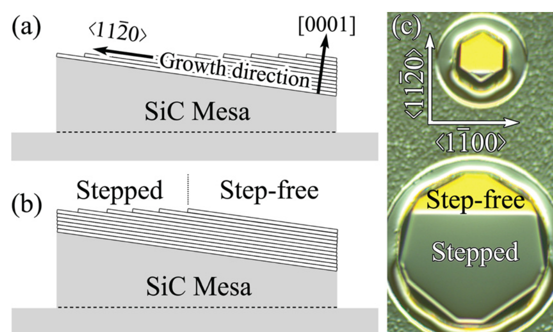

FIG. 1. (Color online) Cartoon of a vicinal SiC mesa (a) before and (b) after step-flow homoepitaxial growth to create a partially step-free surface. (c) A NDIC photograph of two partially step-free mesas with original diameters of 50 μm and 100 μm.

above the surface, is seen in Fig. 1(a). If the homoepitaxial growth time is not long enough to completely grow out the ledges, there is a distinct difference between stepped and step-free regions, as indicated in Fig. 1(b). A Nomarski differential interference contrast (NDIC) photograph of a sample after 60 min of homoepitaxial growth is exhibited in Fig. 1(c). Owing to the anisotropic growth rate of SiC with respect to its crystallographic planes, the mesas themselves change in shape. Their original circular RIE etch shape can still be seen, but the mesa itself has become hexagonal around its perimeter. On the mesa surface, a clear contrast is seen between the stepped and step-free regions. Approximately twenty percent of the 100-μm-diameter mesa is covered by the step-free region and ninety percent coverage is seen on the 50-μm mesa. These coverages are typical for all mesas of this size after 60 min of step-flow growth. For this study, mesas are *purposefully* grown partially step-free to understand the differences between the vicinal, "stepped," regions and the step-free regions that are formed on the exact same mesa. Both regions act as a separate test bed for experiments, which can be performed on a single sample as opposed to requiring separate stepped and step-free samples. Completely step-free mesas can and have been formed, but partially step-free mesas are preferred for this work.

After homoepitaxial growth, atomic force microscopy (AFM) is performed to ensure that the growth was successful in achieving partial step-free coverage and to provide a baseline comparison of the stepped and step-free regions on the mesa surface before thermal decomposition. The AFM profilometry micrographs from the step-free region showed no step features across tens of micrometers, in distinct contrast to the stepped region, which shows step fronts separated by approximately 30 nm. Even 4H-SiC substrates that are cut to be nominally on-axis show steps within a smaller scan area of 5 μm by 5 μm.[8] The AFM used in this study is a Veeco Dimension 3100 with Veeco's TESP model microcantilevers. The AFM is operated in the repulsive tapping mode under a dry nitrogen environment. Both profilometry and phase data are collected and subsequently analyzed with the WSxM software package (v5.0 Develop 1.3).[13]

After ensuring that the step-flow homoepitaxial growth was successful, the step-free substrate is diced into smaller samples. The majority of these samples, each approximately 1 cm^2 in area, are thermally decomposed in a different chamber of the CVD reactor than the one used for the homoepitaxial growth. A few samples are reserved for molten KOH etching, which will be discussed later in this paper. Each thermally decomposed sample is used only once for a single desired growth condition and never reused. Thermal decomposition conditions for this study use a turbo molecular pump to produce a vacuum environment in the low-10^{-5} mbar range at growth temperatures between 1475 °C and 1600 °C. After reaching the desired growth temperature, the sample is held for 10 min before allowing the system to cool under vacuum. Throughout this study, the vacuum environment and 10 min hold time are constant for all thermal decomposition experiments. The only experimental variable is the growth temperature.

To characterize the substrate after graphene synthesis, AFM, Raman spectroscopy, and transmission electron microscopy (TEM) are used. The same AFM measurement conditions are used for characterizing the surface before and after decomposition. Raman spectroscopy is performed using an XploRA model from HORIBA Jobin Yvon with wavelength at 532 nm, under 4 mW of power at the sample, and a lateral resolution of 600 nm. Cross-sectional high-resolution TEM is performed on areas removed from mesas via focused ion beam (FIB) liftout. A single extracted area includes tens of micrometers from both sides of the stepped and step-free regions. The FIB liftout method uses a FEI Nova dual beam FIB/SEM equipped with a Klöcke nanomanipulator.[14] Protective layers of Pt/C are deposited locally, first with the electron beam to avoid surface damage, then followed by a thicker layer deposited using the ion source. TEM micrographs are obtained with an FEI Titan 80-300 operating at 300 kV.

III. RESULTS AND DISCUSSION

A. AFM study

After thermal decomposition at 1475 °C for 10 min, the AFM profilometry micrographs show distinct differences in surface morphology between the stepped and step-free regions of the same mesa, as shown in Figs. 2(a) and 2(b), respectively. Figure 2(a) exhibits the typical stepped profile of a vicinal SiC substrate, with ledges running relatively parallel to each other, and is similar to results found by other researchers.[6,9] Parallel ledges are *not* evidenced on the step-free surface shown in Fig. 2(b). The step-free region is better characterized as having surface features that demonstrate a preference for erosion along symmetry-related low-index planes. However, the preference toward erosion along these planes is slight, because some features, an example being highlighted by the dotted line in Fig. 2(b), deviate from these low-index planes. This deviation appears similar to the finger-like, reconstructed SiC structures found by other researchers[8,15] and qualitatively suggests weak anisotropy in the surface free energy, i.e., shallow cusps in the gamma-plot at the low-index erosion planes.

Figure 2(c) is a derivative image created from an AFM profilometry micrograph of the transition region between the stepped and step-free regions. The contrast contained in the

Downloaded 18 Jul 2013 to 128.46.221.64. This article is copyrighted as indicated in the abstract. Reuse of AIP content is subject to the terms at: http://jap.aip.org/about/rights_and_permissions

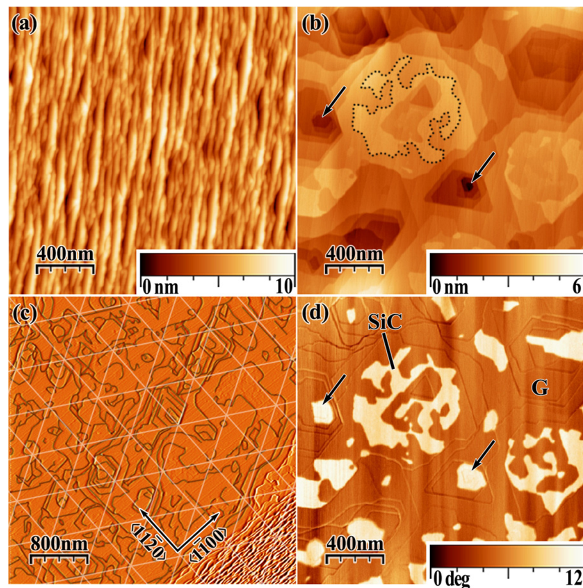

FIG. 2. (Color online) AFM profilometry micrographs of one thermally decomposed, partially step-free mesa contrasting the differences in surface morphology between its (a) stepped region and (b) step-free region. SiC "finger-like" features are highlighted with a dotted line, and two-surface pits are decorated with arrows in (b). (c) Derivative image taken from an AFM profilometry micrograph depicts the transition region between stepped and step-free regions, bottom-right and top-left of the micrograph, respectively. The dark lines on the step-free region highlight surface features with abrupt changes in height, such as ledges. (d) AFM phase micrograph corresponds spatially to (b), with bright areas identified as SiC and dark areas as graphene. Thermal decomposition occurred at 1475 °C for 10 min under vacuum.

image is created by abrupt discontinuities in height from surface features, such as ledges and surface pits. To help highlight the contrast in the step-free region, dark lines are added as a guide for the eye. The derivative image is effective at exhibiting small surface features when the height range of the entire micrograph is much greater than the height of the surface features. Additionally, white solid lines have been overlaid on the image to represent the three-fold symmetry of the SiC$\{1\bar{1}00\}$ planes. On the bottom right of Fig. 2(c), the ledges of the stepped region can be seen running parallel to the SiC$\{11\bar{2}0\}$ planes and appear much like those in Fig. 2(a). Within the step-free region, the surface resembles that of Fig. 2(b). Figure 2(c) shows that the stepped region maintains noticeable striations parallel to the SiC$\{11\bar{2}0\}$ planes, even though the preferred erosion planes for the step-free region are along the SiC$\{1\bar{1}00\}$ planes. This suggests a relatively strong step-step repulsion between the vicinal SiC steps, which maintains the ledges.

Figure 2(d) shows where epitaxial graphene is forming through AFM phase contrast. This phase micrograph corresponds one-to-one spatially with the profilometry micrograph of Fig. 2(b). Previous research with scanning tunneling microscopy has shown that the lighter contrast is indicative of the SiC surface, while the darker region is graphene.[8] Without eroding ledges to seed the initial graphene formation, the step-free region progresses toward graphitization through the expansion of three-fold symmetric surface pits, which are highlighted with arrows in Figs. 2(b) and 2(d). Owing to their three-fold symmetric nature, these features can appear hexagonal or triangular in shape. The formation mechanism causing these pits is different from that of the stepped region, where erosion begins at the step fronts, as expected, but no surface pits are seen. Since they appear to seed graphene formation on the step-free region, understanding the origin of these surface pits is important.

The density of the surface pits for decomposition at the lowest, 1475 °C, and highest, 1600 °C, temperatures studied is approximately the same. A statistical count of the number of pits across ten or more AFM profilometry micrographs from multiple mesas and mesa sizes at each temperature is performed. Regardless of the mesa size or growth temperature, the average pit density on the step-free surface is approximately $1\times10^{8}\text{cm}^{-2}$. This density is far greater than the most prevalent defect in commercial SiC substrates: threading dislocations. Cree SiC substrates have an approximate threading dislocation density of 10^{4} cm^{-2}, which is four orders of magnitude below the calculated pit density.[12,16]

To determine the number of threading dislocations for our substrates, molten KOH etching is performed on a sample that was not thermally decomposed. It has been found that molten KOH etching is an effective means of decorating multiple types of dislocations on the Si-face of SiC. The entire sample is immersed in molten KOH, and etching conditions were similar to those used previously: 520 °C for 20 min in a nickel crucible.[17] Due to the anisotropic KOH etch rate, which is faster at defects as compared to along the basal plane direction, threading dislocations can be easily counted and categorized by optical microscopy. Tens of mesas are analyzed to determine defect density. On the surface of the mesas, a density of approximately $1\times10^{5}\text{cm}^{-2}$ is found, which is within an order of magnitude to the aforementioned threading dislocation value. Furthermore, the defect density was similar for both stepped and step-free regions, indicating that our homoepitaxial step-flow process only increases the defect density by, at most, an order of magnitude. These density values were not affected by mesa size. Overall, there are about three orders of magnitude more surface pits than threading dislocations, which means there are not enough threading dislocations to serve as the origin of every pit.

A more plausible explanation for the formation of the surface pits is stochastic pinning along the periphery of eroding SiC regions. As can be seen in Fig. 2(d), there are two features that are prominently covered by remnants of the original SiC surface. The first are the SiC finger-like features previously discussed and highlighted with a dotted line in Fig. 2(b). The second is at the bottom of the relatively deep pits on the surface, as denoted by arrows in Fig. 2(d). The pits are particularly prominent in Fig. 3 and are, again, highlighted with arrows. These pits seem to resemble the "canyons" found and discussed by Hannon *et al.*[7] Their work, which was performed under UHV and substantially lower decomposition temperatures, elucidated the formation of $\sqrt{3}$ SiC canyons that were caused by the $6\sqrt{3}\times6\sqrt{3}-R30^{\circ}$ SiC buffer layer, pinning the erosion of $\sqrt{3}$ SiC. The shape of these canyons was due in large part to the stepped geometry of their surface, which is markedly different than that of our step-free surface.

Without regularly spaced step fronts eroding, it is found that surface pits are formed through a multistep process.

Downloaded 18 Jul 2013 to 128.46.221.64. This article is copyrighted as indicated in the abstract. Reuse of AIP content is subject to the terms at: http://jap.aip.org/about/rights_and_permissions

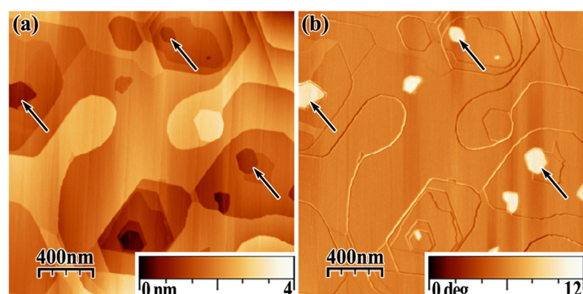

FIG. 3. (Color online) AFM (a) profilometry and (b) phase micrographs of a step-free region after thermal decomposition at 1600 °C for 10 min under vacuum. Arrows point toward a few of the many surface pits eroding along the SiC{$1\bar{1}00$} planes. AFM phase micrograph depicts bright areas as SiC and dark areas as graphene.

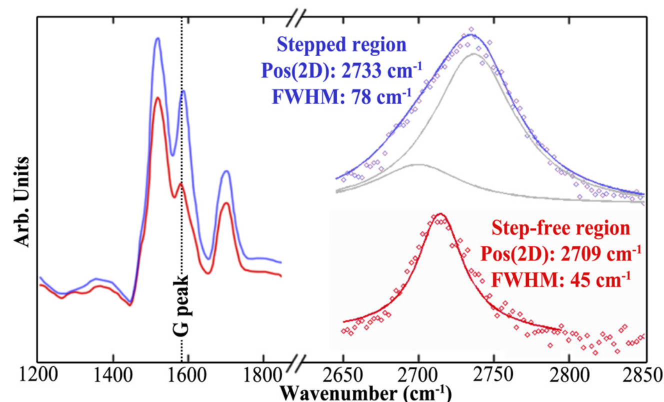

FIG. 4. (Color online) Representative Raman spectra of both stepped (top) and step-free (bottom) regions from the same mesa. The 2D peak is emphasized on the right side of the figure. These spectra are obtained after thermal decomposition at 1475 °C for 10 min.

First, surface vacancies coalesce to form triangular pits on the SiC surface with edges lying along low-index SiC{$1\bar{1}00$} planes. These triangular regions form randomly across the step-free region and serve as non-periodic step fronts, which are analogous to the ledges that are intrinsic to vicinal SiC. Second, as growth temperature or hold time increases,[8] these triangular pits continue to expand through outward erosion, driven by Si sublimation from their edges, and begin to merge. Since the pits nucleate in random locations, this merging creates isolated hexagonal islands of SiC. Finally, this process repeats itself in a fractal-like manner inside the hexagonal SiC islands. Inside this pinned region, vacancies coalesce to form new triangular pits, which then merge, but are contained within the boundaries of the larger island. From stoichiometry, approximately three SiC bilayers need to decompose to form one layer of graphene. Thus, as these nested triangular pits form within each other, the innermost nested pit creates the deepest depression into the substrate as it progresses toward graphitization through the decomposition of three SiC bilayers to form a single layer of graphene. This formation phenomenon leaves SiC at the bottom of the surface pits.

With increasing temperature, the SiC surface features continue to decompose and the surface coverage of graphene increases. A step-free region thermally decomposed at 1600 °C for 10 min is shown in Fig. 3. Figure 3(a) shows a representative AFM profilometry micrograph, and Fig. 3(b) shows a phase contrast micrograph of the same spatial region. The arrows in both micrographs point toward only three of the many surface pits. As can be seen from the AFM phase contrast of Fig. 3(b), the last remaining regions of SiC (lighter contrast) are at the bottom of the surface pits.

As for the finger-like SiC structures exhibited in Fig. 2(b), fewer are seen at the 1600 °C decomposition temperature and none are exhibited in Fig. 3. This is readily apparent in comparing the AFM phase micrographs as thermal decomposition temperature increases. At higher temperature, graphene coverage is more uniform and the areal coverage of SiC is greatly reduced. From a histogram analysis of tens of AFM phase micrographs, the step-free surface is nearly 100% covered with epitaxial graphene after decomposition at 1600 °C. The same analysis shows the surface to be 80% covered with graphene after decomposition at 1475 °C.

B. Raman study

Raman spectroscopy was also used to characterize graphene formed on both stepped and step-free regions. Tens of mesas were analyzed from each growth condition on both the stepped and step-free region. Figure 4 shows representative spectra from a mesa after thermal decomposition at 1475 °C for 10 min. The signature signs of graphene are present: a G peak near 1600 cm^{-1} and a 2D peak around 2700 cm^{-1}. The left side of Fig. 4 depicts a portion of the Raman spectrum, which includes the G peak. Since the G peak is convoluted with SiC resonant peaks, obtaining accurate information about its peak width is difficult. However, the G peak position can be measured and is found to be approximately the same for both stepped and step-free regions. The right side of Fig. 4 shows both raw data points and a fitted curve of the 2D peak for both the stepped and step-free region. A single Lorentzian curve provides the best fit for the step-free region, and a combination of two Lorentzian curves, both shown below the best fit data, estimates the stepped region well.

The 2D peak position and full-width half-maximum (FWHM) for the two regions are distinctly different. The 2D peak position for the stepped region is consistently blue-shifted with respect to the step-free region, and the 2D FWHM of the stepped region is consistently larger. To explore the reason for these differences in Raman peak characteristics, it is important to identify the potential sources of change. There are four variables found to alter the Raman peak characteristics of a graphitic material: laser wavelength,[18,19] carrier concentration,[20–23] strain,[24–26] and film thickness.[27–31]

The first variable, laser wavelength, can be easily ruled out. The same experimental conditions were used for all Raman spectroscopic measurements in this study, including the laser wavelength.

To discredit carrier concentration as a reason for changes to the graphitic Raman peaks, it is assumed that the effect of the substrate vicinal angle is negligible. The carrier concentration for graphene formed on nominally on-axis SiC under identical conditions has been previously found to be n-type with an average density of $2\times10^{12}cm^{-2}$. If carrier

Downloaded 18 Jul 2013 to 128.46.221.64. This article is copyrighted as indicated in the abstract. Reuse of AIP content is subject to the terms at: http://jap.aip.org/about/rights_and_permissions

concentration is comparable to within an order of magnitude for different vicinal angles, then the 2D peak position would not change by more than 5 cm^{-1}.[20] This shift is smaller than that demonstrated in Fig. 4, ruling out the possibility of carrier concentration being the sole cause of the observed disparity between the stepped and step-free 2D peak positions. Additionally, carrier concentration seems to be relatively unaffected by the number of graphene layers. If every layer of graphene contributed equally to conduction, then there would be an increase in carrier concentration as layer thickness increased; however, this effect is not seen.[32]

The third variable that modifies peak characteristics, film strain, shifts both the G and 2D peaks. However, little-to-no shift in the G peak is observed between the stepped and step-free region, nor is there a splitting of the G peak, which is indicative of strain greater than 0.5%.[24] The average difference in the 2D peak position at the 1475 °C growth temperature is 16 cm^{-1}. Depending on the reported value for changing wavenumber with respect to strain,[26] this shift in 2D peak position could represent a minimum strain of 0.3%. This strain is below that needed to split the G peak and would be in reasonable agreement with our measured data; however, strain below 0.5% has been reported to increase the 2D FWHM by, at most, 10 cm^{-1}.[26] This is not a large enough FWHM increase to account for the difference observed. Furthermore, since both stepped and step-free regions are on the same sample, they are thermally decomposed at the same temperature, which means the coefficient of thermal expansion mismatch affects both regions similarly, creating compressive strain.[33] Therefore, strain is concluded *not* to be the predominant variable affecting the Raman peak characteristics.

The fourth variable reported to shift Raman peak characteristics is film thickness. As the number of graphene layers increases, the 2D peak position blueshifts to higher wavenumbers and the FWHM increases;[27,28,30] both phenomena are seen in Fig. 4. On average, the 2D peak position of the stepped region is blueshifted by 16 cm^{-1} with respect to the step-free region. Also, the FWHM for the stepped region is nearly 39 cm^{-1} broader than the step-free region. Given that ledges are a relatively higher surface energy feature that are prone to faster erosion, a thicker graphitic film should be found on regions with more ledges than not. The differences and variability in Raman peak characteristics between stepped and step-free regions are shown in Table I. To test this thickness hypothesis, cross-sectional TEM is performed.

TABLE I. Shape characteristics for the 2D peak position, Pos(2D), and 2D full-width half-maximum, FWHM, as well as the respective standard deviation, σ, are determined from fitting Lorentzian curves to the Raman spectra. Tens of mesas from both stepped and step-free regions are measured at two different growth temperatures.

Growth Temp.	Region	Pos(2D) (cm^{-1})	σ_{Pos} (cm^{-1})	FWHM (cm^{-1})	σ_{FWHM} (cm^{-1})
1475°C	Step-free	2715	4	45	4
	Stepped	2731	1	84	1
1600°C	Step-free	2730	4	60	7
	Stepped	2736	3	83	2

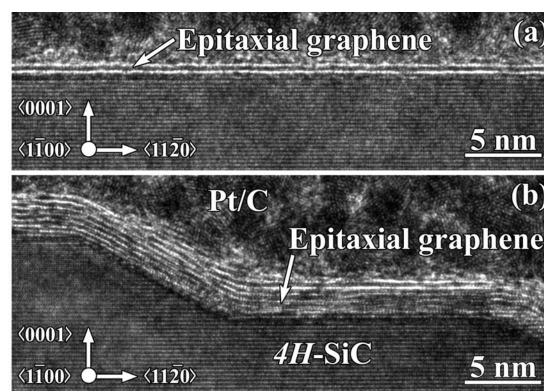

FIG. 5. Cross-sectional high-resolution TEM micrograph showing differences in film thickness between the (a) step-free and (b) stepped regions. Micrographs taken along the SiC$\langle 1\bar{1}00\rangle$ orientation. Thermal decomposition occurred at 1475 °C for 10 min.

Cross-sectional TEM is used to image both the stepped and step-free regions of the same mesa. FIB liftout is performed on the partially step-free, thermally decomposed mesas to extract samples containing both the stepped and step-free regions. Representative TEM micrographs from both regions of a sample thermally decomposed at 1475 °C are exhibited in Fig. 5. The micrographs are imaged along the SiC$\langle 1\bar{1}00\rangle$ direction.

A lack of surface features is depicted in the step-free region imaged in Fig. 5(a). Overall, the step-free region was predominantly covered with 1 to 2 layers of graphene. In contrast, the stepped region shown in Fig. 5(b) shows ledges running more or less parallel to the SiC$\{11\bar{2}0\}$ planes. The graphene film blankets the SiC ledges conformally. The stepped region was consistently covered with 4 to 6 layers of graphene, which is more than twice as thick as the graphene on the step-free region.

Taken together, TEM and Raman spectroscopy provide direct evidence of the effect that film thickness has on Raman peak characteristics. The increase in thickness from the step-free to stepped region corroborates well with the Raman spectroscopy data. An increase in graphene film thickness both blueshifts the 2D peak and increases its FWHM, both of which are seen in Table I.

IV. CONCLUSION

In conclusion, partially step-free SiC mesas have been created through homoepitaxial step-flow growth and subsequently decomposed in vacuum at different temperatures to study graphene formation. Through AFM profilometry, a crystallographic preference for erosion along the SiC$\{1\bar{1}00\}$ planes has been determined on the step-free region, despite vicinal ledges on the stepped region eroding and maintaining their registry along the SiC$\{11\bar{2}0\}$ planes. The density of surface pits has been estimated at $1\times10^{8}\,cm^{-2}$ for samples decomposed at both 1475 °C and 1600 °C, which is three orders of magnitude greater than the measured density of SiC threading dislocations. This orders of magnitude difference indicates that not every pit is formed at a threading dislocation, suggesting that pits are instead formed through localized pinning caused by stochastic geometrical constraints as the edges

Downloaded 18 Jul 2013 to 128.46.221.64. This article is copyrighted as indicated in the abstract. Reuse of AIP content is subject to the terms at: http://jap.aip.org/about/rights_and_permissions

erode across the step-free surface. Raman spectroscopy has elucidated differences in 2D peak shape and position, depending on both the growth temperature and the region being analyzed. This difference is attributed to epitaxial graphene thickness variations, which are caused by a faster erosion rate of vicinal ledges on the stepped regions as compared to the featureless step-free regions. This difference in film thickness is confirmed through cross-sectional TEM measurements.

More research needs to be performed to ascertain the true benefit of using step-free mesas. The stepped regions clearly form a thicker graphitic film than the step-free regions under the exact same growth conditions. Thus, one benefit of using step-free mesas is the broader window of thermal decomposition conditions that can be used due to the slower graphitization rate of the step-free regions. The true value of step-free mesas will need to be determined through the fabrication of electronic devices. The step-free region has a smaller 2D FWHM than the stepped region, which has been correlated to higher Hall mobility values;[34] however, experiments to ascertain mobility values have yet to be performed. Measuring mobility values will help determine the true benefit of the additional fabrication and step-flow growth processes required to form step-free mesas. Furthermore, the use of other thermal decomposition environments, such as argon at near-atmospheric pressure, has been shown to increase Hall mobility values on vicinal surfaces.[10,35] The effect of such a growth environment on the formation mechanism of graphene on step-free SiC surfaces and the subsequent effect on device performance is yet to be determined.

ACKNOWLEDGMENTS

This work is funded by Group 4 Development LLC, Indiana's 21st Century Fund, AFRL, and DARPA.

[1]A. J. Van Bommel, J. E. Crombeen, and A. Van Tooren, Surf. Sci. **48**, 463 (1975).
[2]Y. Q. Wu, P. D. Ye, M. A. Capano, Y. Xuan, Y. Sui, M. Qi, J. A. Cooper, T. Shen, D. Pandey, G. Prakash, and R. Reifenberger, Appl. Phys. Lett. **92**, 092102 (2008).
[3]T. Shen, J. J. Gu, M. Xu, Y. Q. Wu, M. L. Bolen, M. A. Capano, L. W. Engel, and P. D. Ye, Appl. Phys. Lett. **95**, 172105 (2009).
[4]Y.-M. Lin, C. Dimitrakopoulos, K. A. Jenkins, D. B. Farmer, H.-Y. Chiu, A. Grill, and Ph. Avouris, Science **327**, 662 (2010).
[5]T. Kimoto, A. Itoh, H. Matsunami, and T. Okano, J. Appl. Phys. **81**, 3494 (1997).
[6]S. Tanaka, K. Morita, and H. Hibino, Phys. Rev. B **81**, 041406R (2010).
[7]J. B. Hannon and R. M. Tromp, Phys. Rev. B **77**, 241404 (2008).
[8]M. L. Bolen, S. E. Harrison, L. B. Biedermann, and M. A. Capano, Phys. Rev. B **80**, 115433 (2009).
[9]J. Robinson, X. Weng, K. Trumbull, R. Cavalero, M. Wetherington, E. Frantz, M. LaBella, Z. Hughes, M. Fanton, and D. Snyder, ACS Nano **4**, 153 (2010).
[10]K. V. Emtsev, A. Bostwick, K. Horn, J. Jobst, G. L. Kellogg, L. Ley, J. L. McChesney, T. Ohta, S. A. Reshanov, J. Rohrl, E. Rotenberg, A. K. Schmid, D. Waldmann, H. B. Weber, and T. Seyller, Nature Mater. **8**, 203 (2009).
[11]J. A. Venables, *Introduction to Surface and Thin Film Processes* (Cambridge University Press, Cambridge, England, 2000).
[12]J. A. Powell, P. G. Neudeck, A. J. Trunek, G. M. Beheim, L. G. Matus, R. W. Hoffman, Jr., and L. J. Keys, Appl. Phys. Lett. **77**, 1449 (2000).
[13]I. Horcas, R. Fernandez, J. M. Gomez-Rodriguez, J. Colchero, J. Gomez-Herrero, and A. M. Baro, Rev. Sci. Instrum **78**, 013705 (2007).
[14]R. M. Langford and C. Clinton, Micron **35**, 607 (2004).
[15]V. Borovikov and A. Zangwill, Phys. Rev. B **80**, 121406R (2009).
[16]R. E. Stahlbush, K. X. Liu, Q. Zhang, and J. J. Sumakeris, Mater. Sci. Forum **556-557**, 295 (2007).
[17]M. L. Bolen and M. A. Capano, J. Electron. Mater. **38**, 574 (2009).
[18]R. P. Vidano, D. B. Fischbach, L. J. Willis, and T. M. Loehr, Solid State Commun. **39**, 341 (1981).
[19]L. M. Malard, J. Nilsson, D. C. Elias, J. C. Brant, F. Plentz, E. S. Alves, A. H. Castro Neto, and M. A. Pimenta, Phys. Rev. B **76**, 201401(R) (2007).
[20]A. Das, S. Pisana, B. Chakraborty, S. Piscanec, S. K. Saha, U. V. Waghmare, K. S. Novoselov, H. R. Krishnamurthy, A. K. Geim, A. C. Ferrari, and A. K. Sood, Nat. Nanotechnol. **3**, 210 (2008).
[21]J. Yan, Y. Zhang, P. Kim, and A. Pinczuk, Phys. Rev. Lett. **98**, 166802 (2007).
[22]S. Pisana, M. Lazzeri, C. Casiraghi, K. S. Novoselov, A. K. Geim, A. C. Ferrari, and F. Mauri, Nature Mater. **6**, 198 (2007).
[23]V. N. Popov and P. Lambin, Phys. Rev. B **82**, 045406 (2010).
[24]T. M. G. Mohiuddin, A. Lombardo, R. R. Nair, A. Bonetti, G. Savini, R. Jalil, N. Bonini, D. M. Basko, C. Galiotis, N. Marzari, K. S. Novoselov, A. K. Geim, and A. C. Ferrari, Phys. Rev. B **79**, 205433 (2009).
[25]T. Yu, Z. Ni, C. Du, Y. You, Y. Wang, and Z. Shen, J. Phys. Chem. C **112**, 12602 (2008).
[26]G. Tsoukleri, J. Parthenios, K. Papagelis, R. Jalil, A. C. Ferrari, A. K. Geim, K. S. Novoselov, and C. Galiotis, Small **5**, 2397 (2009).
[27]D. S. Lee, C. Riedl, B. Krauss, K. von Klitzing, U. Starke, and J. H. Smet, Nano Lett. **8**, 4320 (2008).
[28]D. Graf, F. Molitor, K. Ensslin, C. Stampfer, A. Jungen, C. Hierold, and L. Wirtz, Nano Lett. **7**, 238 (2007).
[29]C. Faugeras, A. Nerrière, M. Potemski, A. Mahmood, E. Dujardin, C. Berger, and W. A. de Heer, Appl. Phys. Lett. **92**, 011914 (2008).
[30]A. Gupta, G. Chen, P. Joshi, S. Tadigadapa, and P. C. Eklund, Nano Lett. **6**, 2667 (2006).
[31]A. C. Ferrari, J. C. Meyer, V. Scardaci, C. Casiraghi, M. Lazzeri, F. Mauri, S. Piscanec, D. Jiang, K. S. Novoselov, S. Roth, and A. K. Geim, Phys. Rev. Lett. **97**, 187401 (2006).
[32]J. Kedzierski, P.-L. Hsu, P. Healey, P. W. Wyatt, C. L. Keast, M. Sprinkle, C. Berger, and W. A. de Heer, IEEE Trans. Electron Devices **55**, 2078 (2008).
[33]G. Prakash, M. A. Capano, M. L. Bolen, D. Zemlyanov, and R. G. Reifenberger, Carbon **48**, 2383 (2010).
[34]M. L. Bolen, T. Shen, J. J. Gu, R. Colby, E. A. Stach, P. D. Ye, and M. A. Capano, J. Electron. Mater. **39**, 2696 (2010).
[35]J. L. Tedesco, B. VanMil, R. L. Myers-Ward, J. Culbertson, G. Jernigan, P. Campbell, J. M. McCrate, S. A. Kitt, C. Eddy, Jr., and D. K. Gaskill, ECS Trans. **19**, 137 (2009).

Downloaded 18 Jul 2013 to 128.46.221.64. This article is copyrighted as indicated in the abstract. Reuse of AIP content is subject to the terms at: http://jap.aip.org/about/rights_and_permissions